Preprint
UCRL-JC-141084-REV-1

3D HYDRA Simulations of NIF Targets

M. M. Marinak, G. D. Kerbel, N. A. Gentile, O. Jones, D. Munro, S. Pollaine, T. R. Dittrich, S. W. Haan

This article was submitted to the 42nd Annual Meeting of the APS Division of Plasma Physics, Quebec City, Canada, October 23-27, 2000

U.S. Department of Energy

Lawrence
Livermore
National
Laboratory

October 30, 2000

This work was performed under the auspices of the United States Department of Energy by the University of California, Lawrence Livermore National Laboratory under contract No. W-7405-Eng-48.

This work was performed under the auspices of the United States Department of Energy by the University of California, Lawrence Livermore National Laboratory under contract No. W-7405-Eng-48.

3D HYDRA simulations of NIF targets

M. M. Marinak, G. D. Kerbel, N. A. Gentile, O. Jones,

D. Munro, S. Pollaine, T. R. Dittrich, S. W. Haan

Lawrence Livermore National Laboratory

(October 30, 2000)

Abstract

The performance of NIF target designs is simulated in three dimensions using the HYDRA multiphysics radiation hydrodynamics code. In simulations of a cylindrical NIF hohlraum that include an imploding capsule, all relevant hohlraum features and the detailed laser illumination pattern, the motion of the wall material inside the hohlraum shows a high degree of axisymmetry. Laser light is able to propagate through the entrance hole for the required duration of the pulse. Gross hohlraum energetics mirror the results from an axisymmetric simulation. A NIF capsule simulation resolved the full spectrum of the most dangerous modes that grow from surface roughness. Hydrodynamic instabilities evolve into the weakly nonlinear regime. There is no evidence of anomalous low mode growth driven by nonlinear mode coupling.

I. INTRODUCTION

The National Ignition Facility, under construction, is a 192 beam frequency tripled ($\lambda = 0.35\mu m$) Nd:glass laser system designed to generate shaped pulses delivering 1.8 MJ at a peak power of 500 TW. Detailed computer simulations have been performed for a variety of indirectly-driven targets designed to achieve ignition on NIF. [1–8] These designs employ a cylindrical hohlraum which converts laser light to x-rays, resulting in a more symmetric drive on the capsule. The hohlraum designs have been modelled extensively with the 2-D multiphysics radiation hydrodynamics code LASNEX. [9] The large number of beams on NIF are intended to produce a nearly axisymmetric radiation flux onto the capsule. There exist, however, a number of issues one would like to examine with direct 3-D simulations. These include the possibility that the discrete laser spots cause significant azimuthal asymmetries in the wall motion. Such an asymmetry might affect implosion symmetry hydrodynamically or by generating asymmetries in the radiation flux. The ability to keep the laser entrance hole open in the absence of an axisymmetric illumination pattern should also be assessed. A direct 3-D hohlraum simulation allows us to calculate the radiation flux on the capsule taking into full account such effects as wall motion, laser spot broadening, albedo variations and volumetric emission from the hohlraum channel.

In addition to the asymmetry caused by the radiation drive, perturbations on the capsule surfaces seed hydrodynamic instabilities, which can cause shell breakup and quench capsule ignition. For a broad range of modes the growth factors due to hydrodynamic instabilities are sufficiently large that perturbations progress into the nonlinear regime, where saturation effects and mode coupling are important. The higher nonlinear saturation amplitudes obtained in three dimensions are well established. [10–16] Besides assessing a capsule's ability to withstand these larger amplitudes, we wish to examine the effects of nonlinear mode coupling in the presence of the full spectrum of modes. We are interested in whether nonlinear mode coupling between high order modes generates low mode asymmetries which could threaten ignition.

This article presents examples of how HYDRA is being used to simulate in three dimensions these aspects of the targets designed for the NIF. The remainder of this article is organized as follows. In Section II we describe HYDRA. A description of the hohlraum simulation results is presented in Section III. We discuss in Section IV results from a highly resolved, large solid angle simulation of hydrodynamic instabilities on a NIF ignition capsule.

II. HYDRA

HYDRA is a 2D and 3D multiphysics radiation hydrodynamics code. It now has the essential physics required for simulations of NIF targets. HYDRA is based upon Arbitrary Lagrange Eulerian (ALE) hydrodynamics, employing modern monotonic artificial viscosities to stabilize shocks. A variety of algorithms are available for controlling grid motion, including weighted equipotential relaxation. Second order monotonic advection is performed on scalar fields and momentum. Material interfaces are resolved using interface reconstruction. [17] HYDRA includes a laser raytrace and deposition package that calculates ray orbits with second order accuracy and includes ponderomotive effects. A heavy ion deposition package is available. Radiation transport is handled either with Monte Carlo photonics or with flux limited multigroup diffusion. A variety of LTE and NLTE opacity models are available, including inline XSN [18], and the newly developed Linear Response Matrix Opacity method for NLTE opacities [19]. An online server allows LTE opacity tables to be generated for arbitrary mixtures. Electron and ion conduction are treated using flux-limited finite element diffusion operators. Conductivities and electron-ion coupling coefficients are obtained from the model of Lee and More [20].

Modelling of thermonuclear burn includes multigroup charged particle transport and isotope production and depletion. Neutron energy deposition can be treated adequately in the free streaming limit for ICF capsules, which are thin to neutrons. A variety of methods are available for solving matrices which arise from the operator splitting employed. For large matrices two scaleable multigrid methods are available from the HYPRE [21] solver

library. Many equations of state are available, including the inline Quotidian equation of state (QEOS), the EOS IV tabular data base, Sesame tables and the LEOS library.

HYDRA has been modified to run on distributed clustered SMP architectures, using a strategy based upon POSIX threads, OpenMP and the MPI message passing library. High parallel performance has demonstrated on problems using up to 1680 processors of the ASCI SKY machine at Lawrence Livermore National Laboratory. HYDRA has been used in the design and simulation of a range of laser-driven experiments. [15,22,23]

III. HOHLRAUM SIMULATIONS

We first consider a scale 0.6 hohlraum which was designed for the 96 beam configuration initially planned for NIF. A schematic of the target is shown in figure 1. The hohlraum measures 6.0 mm long by 3.3 mm in diameter. A gas fill mixture of equal amounts of He-H at 6×10^{-4} g/cm^3 is intended to control the motion of the hohlraum wall material. A 0.8 μm thick polyimid window on each laser entrance hole maintains the gas fill. The hohlraum wall is fabricated from a mixture of equal amounts of U-Pb-Ta-Dy-Nb. This "cocktail" mixture is designed to yield higher energy conversion efficiency than pure gold hohlraums. A plastic liner covers the high-Z wall material at the laser entrance hole. The capsule has a polyimid ablator ($C_{22}H_{10}N_2O_4$) 95 μm thick enclosing a cryogenic layer of DT 48 μm thick. The center of the capsule contains DT gas at a density of 0.3 mg/cm^3.

We simulated 1/4 of the hohlraum with two symmetry planes, one at the equator and one running through the hohlraum axis. The simulation models all of the hohlraum features described above. For the purposes of this simulation the hohlraum was illuminated using the 192 beam pattern of full NIF. Light comes into the laser entrance hole in two cones. The inner cone is composed of beams aimed at 23.5 and 30 degrees to the hohlraum axis, and the other has beams at 44.5 and 50 degrees. The 48 beams which enter the quarter hohlraum are aimed at 12 locations and are represented by twelve beams in the calculation. Eight of these groups are associated with the outer cone. Each beam group is represented

in the laser package by 300 rays, with an elliptical focal spot. The relative power in the cones is dynamically varied during the 10.0 ns pulse to minimize the time-varying pole-to-waist asymmetry, which is described as a P_2 Legendre polynomial. At the time of this writing the Monte Carlo photonics package did not yet function with the material interface tracker. This simulation was performed using multigroup radiation diffusion, inline XSN LTE opacities [18], and the Quotidian equation of state. The laser beams are the significant source of 3-D asymmetries in the hohlraum wall and channel. Energy losses from the laser hot spots, due to conduction and radiation emission, are expected to be calculated with reasonable accuracy using this model.

Figures 2a-c shows the electron temperature contours on a cut-away view of a mesh surface inside the hohlraum for three times. The laser beams burn through the polyimid window and then into the gas for 900 ps before the outer ring begins heating the wall appreciably. Initially individual laser spots are visible. These laser spot quickly broaden, converting the contours at the outer cone into a true ring pattern. The beams forming the inner ring reach the wall at 2.2 ns. Due to the smaller number of beams and the approximation of reflection symmetry about the equator the laser hot spots in the inner ring remain more distinct than for the outer ring. By the last time shown, the electron temperature has evolved to a very high degree of azimuthal symmetry, as expected.

Figures 3a-c plots the motion of the various material regions on the boundaries of the simulated volume for three times. The plastic liner around the laser entrance hole ablates into the surrounding volume, delaying the arrival of the high-Z hohlraum wall material, as shown in Fig. 3b. It succeeds in keeping the hole open for the required duration of the laser pulse. The hole closes by the last time shown, after the required energy has been delivered and the capsule has fully converged.

The density profile in the interior of the hohlraum shows the gas effectively controls the wall motion. Only slight deviations from axisymmetry occur in the density profile in the main hohlraum volume. These variations are largest in the vicinity of the laser entrance hole. The energetics from this hohlraum have been compared with a 2-D axisymmetric simulation.

The radiation temperatures obtained from these simulations are nearly identical.

The radiation diffusion approximation results in an artificially symmetric flux of radiation onto the capsule. Accordingly the capsule maintains a very high degree of spherical symmetry, after converging by more than a factor of 30. The indicates that the hohlraum generates no significant 3-D hydrodynamic asymmetry that effects the capsule. This particular target design is not intended to ignite the capsule, which produces a yield of 4 kJ.

The radiation flux onto the capsule can be obtained from the 3D hohlraum simulations. The transport equations are integrated directly on rays which foliate 2π solid angle at locations on the capsule surface. This method takes into account the convergence of the capsule during the implosion.

Three-dimensional components of asymmetry can also be calculated using a viewfactor code. Those calculations allow for the time variation in the wall albedo and the capsule convergence. But the viewfactor analysis lacks potentially important effects such as volumetric emission and laser spot broadening due to thermal conduction.

We have calculated the intrinsic radiation flux from the quarter hohlraum simulation. We note that the approximations to the illumination pattern introduced by the symmetry planes are quite significant. The symmetry plane at the equator modifies the illumination pattern to intensify the inner cone laser spots on the equator. We have compared coefficients obtained with the two approaches outlined for the spherical harmonic modes that have significant amplitudes. For the effective illumination geometry of this simulation these modes are Y_{44}, Y_{64}, Y_{84} and Y_{88}. In spite of the physical effects omitted by the viewfactor code analysis, the two methods produce a similar picture of the 3-D intrinsic radiation asymmetries in this problem. These techniques give us the capability to calculate radiation flux inside the hohlraum from a direct 3-D simulation. We can impose this radiation flux on the capsule and assess its effect on implosion symmetry. In the future we will employ these techniques in full hohlraum simulations using the exact NIF illumination geometry.

IV. MODELLING OF HYDRODYNAMIC INSTABILITIES

We study hydrodynamic instability growth by performing highly resolved simulations of a subset of the capsule solid angle. These treat nonlinear saturation and mode coupling [15,16,23–25] in the presence of spherical convergence. We are interested in simulating the growth of the full spectrum of dangerous modes simultaneously to assess whether nonlinear mode coupling between high modes in the ablator drives up low modes, which could affect the capsule's performance. Advances in the computing power available under the Accelerated Strategic Computing Initiative (ASCI) program have enabled us to model considerably larger solid angles than was previously practical. [8]. We consider here a simulation with a domain extending from -36 to +36 degrees in latitude and 72 degrees in longitude. The mesh measured 360 x 360 x 171 zones in the two transverse directions and radial direction respectively. The mesh motion algorithm ensures 0.7 μm radial zone spacing for all regions of the capsule shell that have interacted with the first shock. It has 18 transverse zones per wavelength for $l = 100$. This mesh can resolve the growth of modes with $l \sim$ 2-100 with good accuracy. Above l=100 the product of amplitude with growth factor is small enough that these modes should make only a small contribution to the resulting ablation front rms amplitude. Previous 2-D multimode simulations that included modes up to l=160 support this conclusion. Therefore, we believe this simulation resolves the full spectrum of the most dangerous modes which arise from surface roughness.

Fig. 4 shows a schematic of the capsule simulated, which employs a beryllium ablator doped with 0.9 % copper (BeCu). Its design parameters were specified by Dittrich. [4] It is a variation of a design by Wilson. [3] Other beryllium capsule designs have been proposed. [1] The ablator is 135 μm thick, extending to an outer capsule radius of 1085 μm. Dopants in the ablator shield the fuel from x-ray preheat and help to reduce the Atwood number at the ablator-fuel interface, reducing small scale instability growth there. The 80 μm thick cryogenic DT ice region inside of the ablator encloses a region of DT gas in equilibrium with the ice. The design is driven by a shaped pulse, with a peak temperature of 300 ev produced

by the full 192 beam configuration of NIF. The laser power history used to drive this capsule has four steps, designed to maintain the fuel on a low adiabat.

The tolerances for surface roughness are by far most restrictive on the outer ablator and inner ice surfaces. [5–8]. We initialized the perturbations on the gas-ice surface based upon laboratory measurements. [26] The surface perturbations were described with a functional form:

$$R_{lm}(cm) = \frac{1.0 \times 10^{-4}}{3l^{0.6} + 2.2 \times 10^{-7} l^4}$$

where R_{lm} is the spherical harmonic perturbation amplitude in centimeters and l is the perturbation mode number. Recent work on this surface and its characterization shows smaller mode amplitudes than were used here. The form of the spectrum used for the beryllium copper ablator is as the same as given in ref. [5]

The imposed perturbations have the form

$$G(\theta, \phi) = \sum_m \sum_n a_{mn} cos(\frac{m\pi\theta}{\Delta\theta}) cos(\frac{n\pi\phi}{\Delta\phi}),$$

where a_{mn} is the mode coefficient. Reflection boundary conditions are employed at the transverse boundaries. The power in the 3D spectrum is summed into bins and distributed to the discreet modes supported which have the closest effective l values up to 100. Random phasse factors are assigned to a_{mn} so that the topology of the surface does not have uncharacteristically large peaks and valleys. Contour plots of the actual perturbations initilized on the surfaces are shown in Fig. 5a,b.

Fig. 6 shows two iso-density contour surfaces from the simulation at 15.55 ns, near the time of peak implosion velocity. These surfaces are in the ablator and the inner boundary of the capsule wall. The prominent bubbles and spike sheets growing in the ablation front are described by mode numbers l=60-90. Fig. 7 shows similar surfaces at 15.65 ns, after the capsule has reached peak implosion velocity. The ratio of amplitude to wavelength in the ablator has increased largely due to the effect of convergence. The basic perturbation pattern persists through the implosion phase, indicating weakly nonlinear behavior. For

implosions which successfully ignite, as does the present example, bubble merger [27] is not a prominent feature in ablation front evolution. But nonlinear saturation and mode coupling are important. These high modes growing in the ablator can threaten shell integrity during the implosion phase, when the shell is thinnest, if they breach it before the peak implosion velocity is attained. In spite of the apparently large amplitudes in the ablator in Fig. 5, these perturbations can no longer reach the inside of the capsule as it rapidly thickens due to convergence. Bubbles rising on the inner shell surface have widths associated with a much lower range of mode numbers, falling in the range l = 10-20. The topology of the growing perturbations remains similar across the solid angle. There is no indication of significant low mode asymmetries driven by mode coupling. The capsule produces a robust yield of 15.4 MJ, compared with a 1-D clean yield of 17.0 MJ. The yield, along with the amplitudes and mode numbers of the dominant features in the capsule shell, resemble results from previous 3D simulations performed over a 12 degree wedge with similar initial amplitudes, [8] indicating those simulations were able to model the important nonlinear dynamics of the instability growth.

V. CONCLUSIONS

HYDRA can now model many aspects of NIF target performance in three dimensions. Initial simulations of gas filled cylindrical hohlraums, including the capsule implosion, showed gas fill effectively controlled the hohlraum wall motion, which exhibited little deviation from axisymmetry in the main volume. For parameters used in these calculations the laser entrance hole did remain open for the required duration of the laser pulse. The radiation temperature in the hohlraum was essentially identical to the results for an equivalent 2D axisymmetric simulation performed with HYDRA.

A highly resolved, large solid angle simulation of a NIF capsule modelled the growth of the full spectrum of the most dangerous modes caused by surface roughness. Hydrodynamic instabilities evolved into the weakly nonlinear regime. There was no evidence anomalous

low mode growth driven by nonlinear mode coupling.

ACKNOWLEDGEMENTS

This work was performed under the auspices of the U.S. Department of Energy by the University of California Lawrence Livermore National Laboratory under contract W-7405-Eng-48.

REFERENCES

[1] J. D. Lindl, Phys. Plasmas **2**, 3933 (1995)

[2] S. W. Haan, S. M. Pollaine, J. D. Lindl, L. J. Suter, R. L. Berger, L. V. Powers, W. E. Alley, P. A. Amendt, J. A. Futterman, W. K. Levedahl, M. D. Rosen, D. P. Rowley, R. A. Sacks, A. I. Shestakov, G. L. Strobel, M. Tabak, D. B. Harris, N. M. Hoffman, and B. H. Wilde, Phys. Plasmas **2**, 2480 (1995).

[3] W. J. Krauser, N. M. Hoffman, D. C. Wilson, B. H. Wilde, W. S. Varnum, D. B. Harris, F. J. Swenson, P. A. Bradley, S. W. Haan, S. M. Pollaine, A. S. Wan, J. C. Moreno, P. A. Amendt, Phys. Plasmas **3**, 2084 (1996).

[4] T. R. Dittrich, S. W. Haan, S. Pollaine, A. K. Burnham, G. L. Strobel, Fusion Tech. **31** (4) (1997).

[5] T. R. Dittrich, S. W. Haan, M. M. Marinak, S. M. Pollaine, and R. McEachern, Phys. Plasmas **5**, 3708 (1998).

[6] T. R. Dittrich, S. W. Haan, M. M. Marinak, S. M. Pollaine, D. E. Hinkel, D. H. Munro, C. P. Verdon, G. L. Strobel, R. McEachern, R. C. Cook, C. C. Roberts, D. C. Wilson, P. A. Bradley, L. R. Foreman, and W. S. Varnum, Phys. Plasmas **6**, 2164 (1999).

[7] D. C. Wilson, P. A. Bradley, N. M. Hoffman, F. J. Swenson, D. P. Smitherman, R. E. Chrien, R. W. Margevicius, D. J. Thoma, L. R. Foreman, J. K. Hoffer, S. R. Goldman, S. E. Caldwell, T. R. Dittrich, S. W. Haan, M. M. Marinak, S. M. Pollaine, J. J. Sanchez, Phys. Plasmas **5**, 1953 (1998).

[8] M. M. Marinak, S. W. Haan, T. R. Dittrich, R. E. Tipton, G. B. Zimmerman **5**, 1125 (1998).

[9] G. B. Zimmerman and W. L. Kruer, Comments Plasma Phys. Control. Fusion **2**, 51 (1975).

[10] G. Tryggvason and S. O. Unverdi, Phys. Fluids A **2**, 656 (1990).

[11] T. Yabe, H. Hoshino, and T. Tsuchiya, Phys. Rev. A **44**, 2756 (1991).

[12] H. Sakagami and K. Nishihara, Phys. Rev. Lett. **65**, 432 (1990).

[13] R.P.J. Town and A.R. Bell, Phys. Rev. Lett. **67**, 1863 (1991).

[14] J.P. Dahlburg *et al.*, Phys. Fluids B **5**, 571 (1993).

[15] M.M. Marinak, B.A. Remington, S.V. Weber, R.E. Tipton, S.W. Haan, K.S. Budil, O.L. Landen, J.D. Kilkenny, and R. Wallace, Phys. Rev. Lett. **75**, 3677 (1995).

[16] J. Hecht, U. Alon, and D. Shvarts, Phys. Fluids **6**, 12 (1994); J. Hecht *et al.*, Laser Part. Beams **13**, 423 (1995); D. Shvarts *et al.*, Phys. Plasmas **2**, 2465 (1995).

[17] D.L. Youngs, in *Numerical Methods for Fluid Dynamics*, edited by K.W. Morton and M.J. Baines (Academic, New York, 1982), p. 273.

[18] See National Techical Information Service Document No. UCRL-52276 (W.A. Lokke and W.H. Grasberger, in Lawrence Livermore National Laboratory Report No. UCRL-52276, 1977). Copies may be ordered from National Technical Information Service, Springfield, VA 22161; G.B. Zimmerman and R.M. More, J. Quant. Spectrosc. Radiat. Transf. **23**, 517 (1980); R.M. More, *ibid.* **27**, 345 (1982).

[19] R. More, T. Kato, Phys. Rev. Lett., **81**, 814 (1998).

[20] Y.T. Lee and R.M. More, Phys. Fluids **27**, 1273 (1984).

[21] P. N. Brown, R. D. Falgout, J. E. Jones, SIAM J. Sci. Comput. (1999).

[22] M.M. Marinak, R.E. Tipton, O.L. Landen, T.J. Murphy, P. Amendt, S.W. Haan, S.P. Hatchett, C.J. Keane, R. McEachern, and R. Wallace, Phys. Plasmas **3** 2070 (1996).

[23] M.M. Marinak, S.G. Glendinning, R.J. Wallace, B. A. Remington, K.S. Budil, S.W. Haan, R.E. Tipton, and J.D. Kilkenny, Phys. Rev. Lett. **80** 4426 (1998).

[24] R.J. Taylor J.P. Dahlburg, A. Iwase, J.J. Gardner, D.E. Fyfe, and O. Willi, Phys. Rev. Lett. **75**, 3677 (1995).

[25] J.P. Dahlburg, D.E. Fyfe, J.H. Gardner, S.W. Haan, S.E. Bodner, and G.D. Doolen, Phys. Plasmas **2**. 2453 (1995).

[26] J.K. Hoffer, L.R. foreman, J. J. Sanchez, E.R. Mapoles, and J. D. Sheliak, Fusion Technol, **30**, 529 (1996).

[27] U. Alon, D. Shvarts, and D. Mukamel, Phys. Rev. E **48**, 1008 (1993); Phys. Rev. Lett. **72**, 2867 (1994).

FIGURES

FIG. 1. Schematic of the gas-filled scale 0.6 cocktail hohlraum.

FIG. 2. Electron temperature on a cut-away view of mesh surfaces at (a) 1.0 ns, (b) 1.75 ns and (c) 5.75 ns.

FIG. 3. Motion of hohlraum materials shown on simulation boundaries at (a) 1.0 ns, (b) 7.0 ns and (c) 10.25 ns. Hohlraum wall is cyan, plastic liner is dark blue, He-H gas fill is purple, polyimid window and ablator are green and DT is red.

FIG. 4. Schematic of copper-doped beryllium ablator capsule.

FIG. 5. Plots of surface perturbations placed on (a) inner ice and (b) outer ablator surfaces.

FIG. 6. Density iso-contour surfaces of 13.8 g/cm^3 at 15.55 ns. These bound the capsule shell.

FIG. 7. Density iso-contour surfaces of 45 g/cm^3 at 15.65 ns.

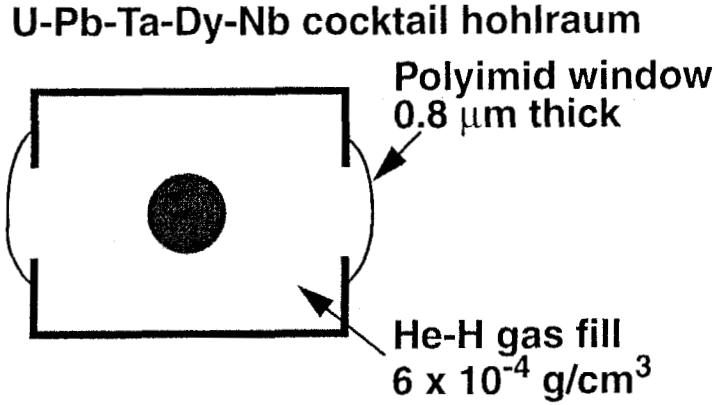
U-Pb-Ta-Dy-Nb cocktail hohlraum
Polyimid window
0.8 μm thick
He-H gas fill
6 x 10-4 g/cm3

Fig. 1

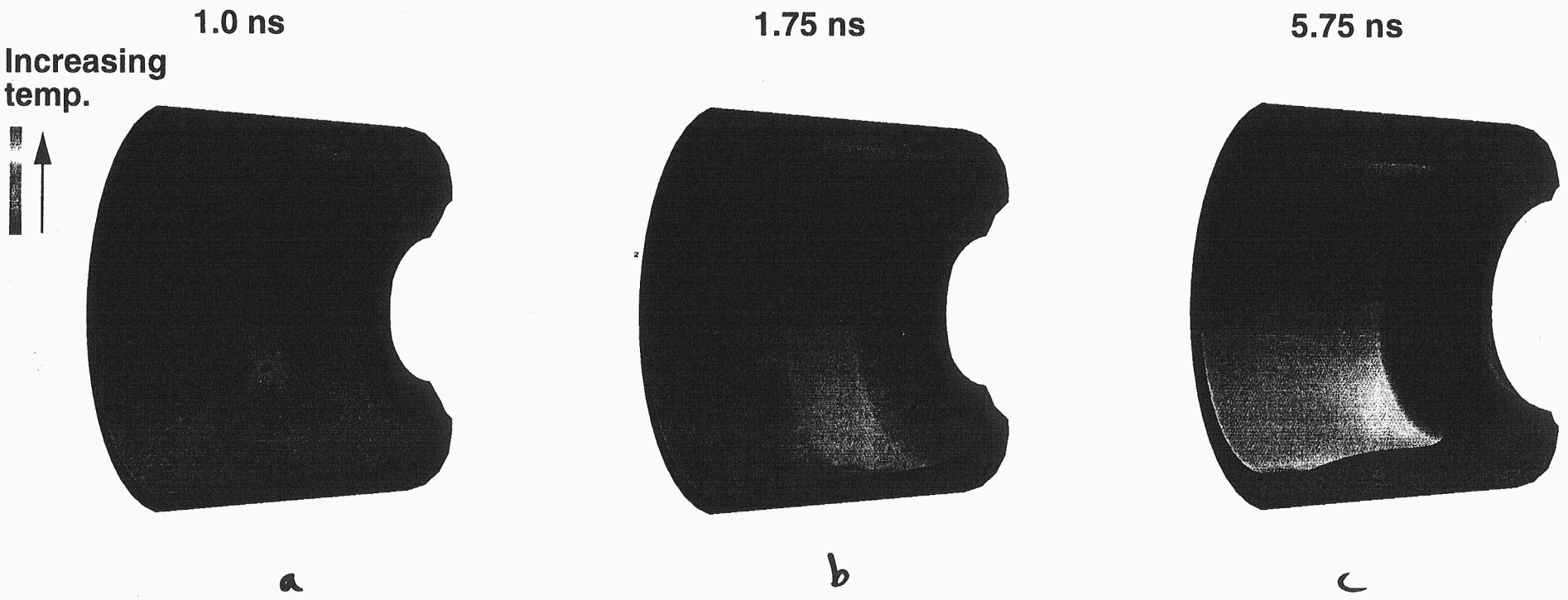

Fig. 2

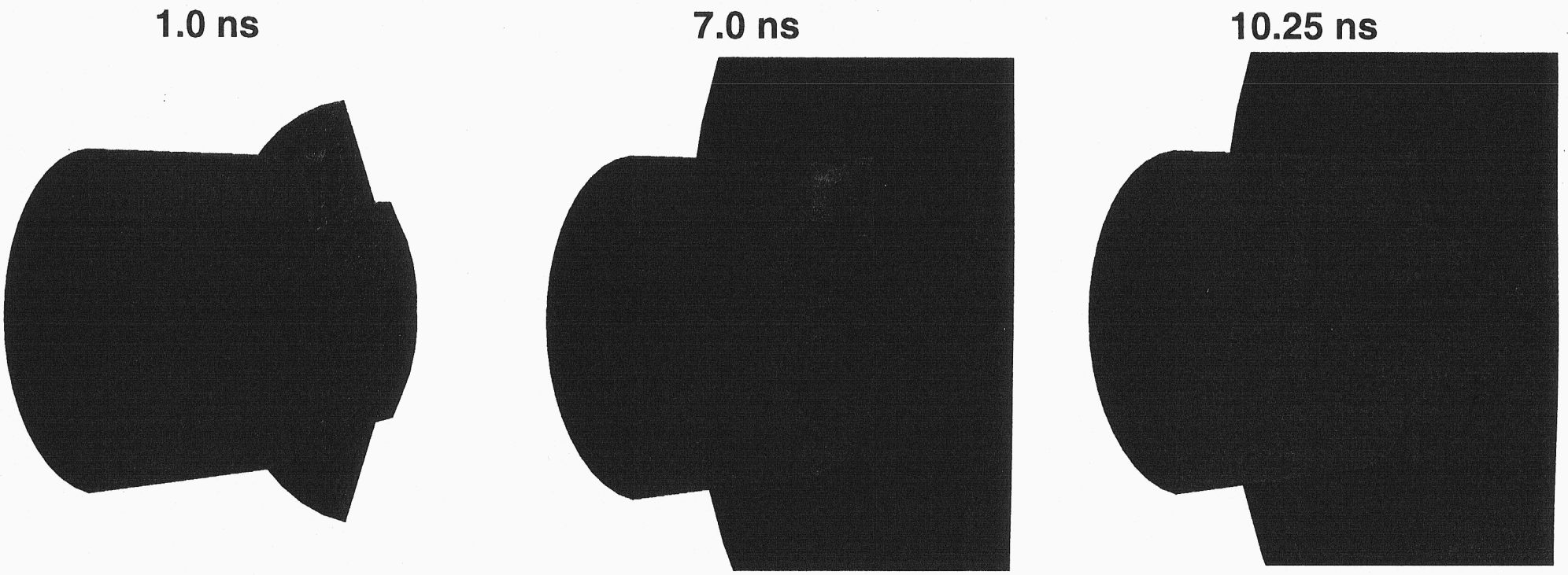

Fig.3

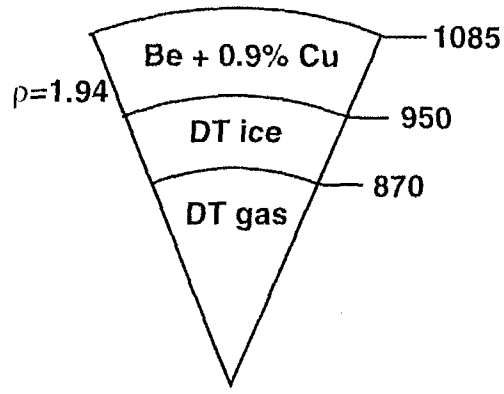
Copper-doped
beryllium ablator
Be + 0.9% Cu
ρ=1.94
DT ice
DT gas
1085
950
870

Fig. 4

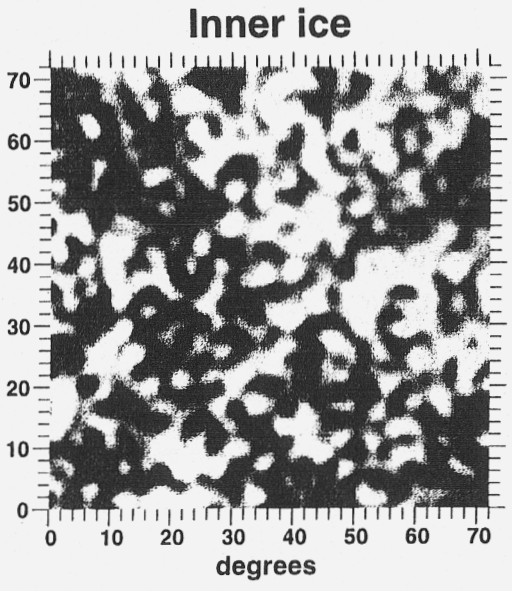
Inner ice
70
60
50
40
30
20
10
0
0 10 20 30 40 50 60 70
degrees

a

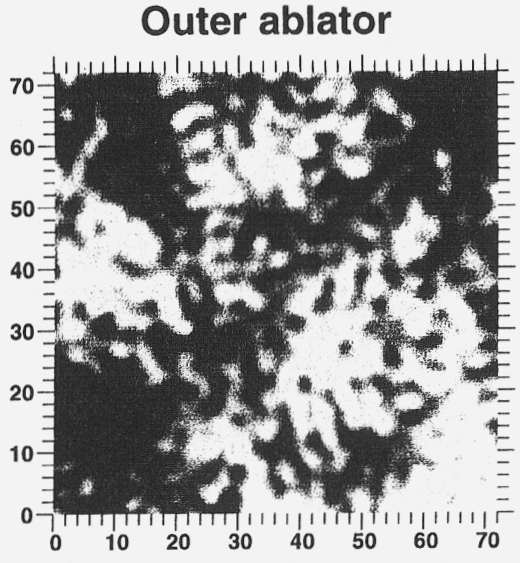
Outer ablator
70
60
50
40
30
20
10
0
0 10 20 30 40 50 60 70

b

Fig. 5

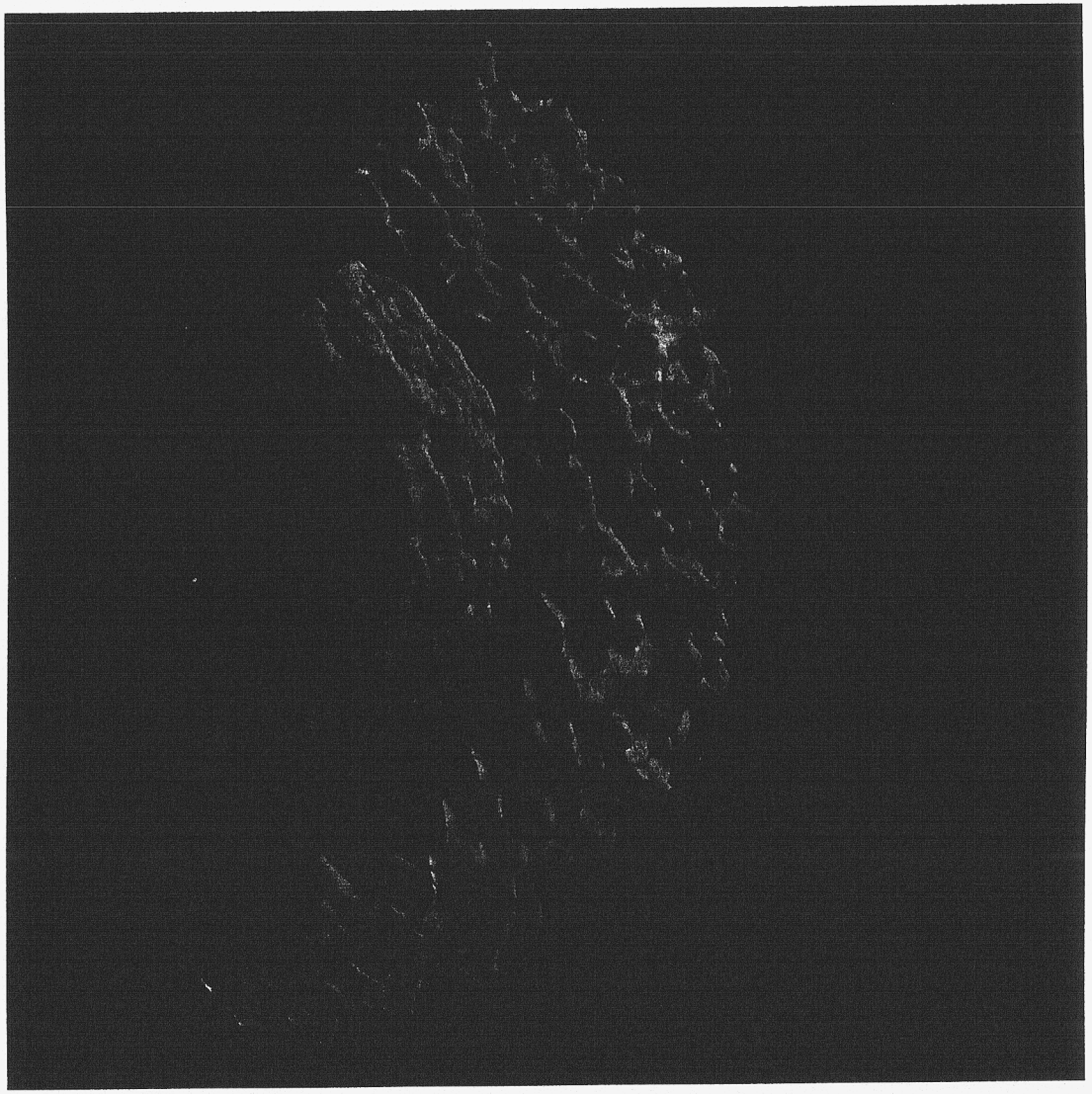

Fig. 6

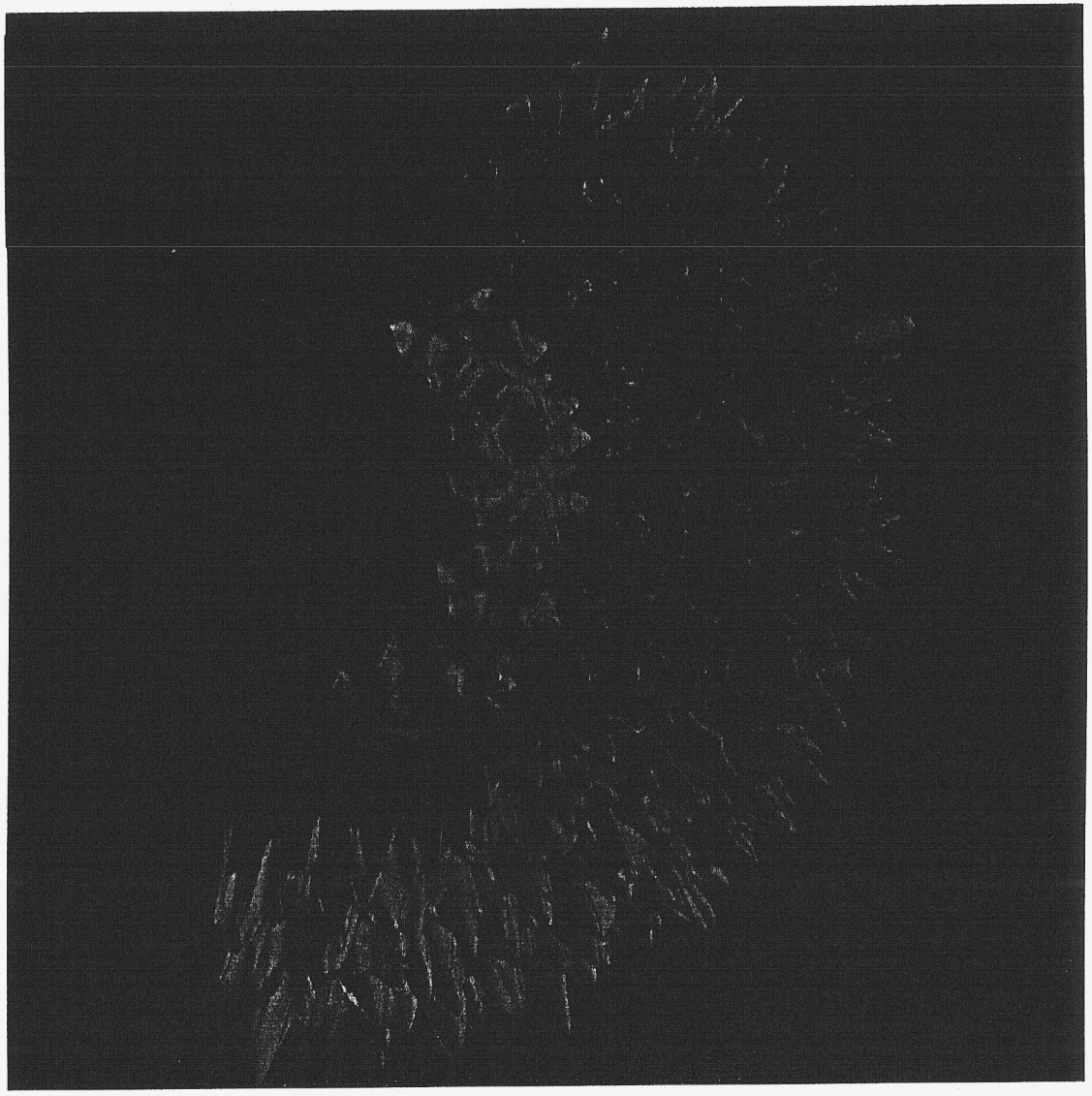

F.g. 7